Original Article

JCBFM

Journal of Cerebral Blood Flow & Metabolism
2018, Vol. 38(3) 422–432

DOI: 10.1177/0271678X17694905
journals.sagepub.com/home/jcbfm
SAGE

Recurrence of glioblastoma is associated with elevated microvascular transit time heterogeneity and increased hypoxia

Andreas Stadlbauer[1,2], Kim Mouridsen[3], Arnd Doerfler[4], Mikkel Bo Hansen[3], Stefan Oberndorfer[5], Max Zimmermann[1], Michael Buchfelder[1], Gertraud Heinz[2] and Karl Roessler[1]

Abstract

Dynamic susceptibility contrast (DSC) perfusion MRI provide information about differences in macro- and microvasculature when executed with gradient-echo (GE; sensitive to macrovasculature) and spin-echo (SE; sensitive to microvasculature) contrast. This study investigated whether there are differences between macro- and microvascular transit time heterogeneity (MVTH and μVTH) and tissue oxygen tension ($PO2_{mit}$) in newly-diagnosed and recurrent glioblastoma. Fifty-seven patients with glioblastoma (25 newly-diagnosed/32 recurrent) were examined with GE- and SE-DSC perfusion sequences, and a quantitative blood-oxygen-level-dependent (qBOLD) approach. Maps of MVTH, μVTH and coefficient of variation (MCOV and μCOV) were calculated from GE- and SE-DSC data, respectively, using an extended flow-diffusion equation. $PO2_{mit}$ maps were calculated from qBOLD data. Newly-diagnosed and recurrent glioblastoma showed significantly lower ($P \leq 0.001$) μCOV values compared to both normal brain and macrovasculature (MCOV) of the lesions. Recurrent glioblastoma had significantly higher μVTH ($P = 0.014$) and μCOV ($P = 0.039$) as well as significantly lower $PO2_{mit}$ values ($P = 0.008$) compared to newly-diagnosed glioblastoma. The macrovasculature, however, showed no significant differences. Our findings provide evidence of microvascular adaption in the disorganized tumor vasculature for retaining the metabolic demands in stress response of therapeutically-uncontrolled glioblastomas. Thus, μVTH and $PO2_{mit}$ mapping gives insight into the tumor microenvironment (vascular and hypoxic niches) responsible for therapy resistance.

Keywords

Glioblastoma, microvasculature, oxygen-tension, recurrence, transit-time-heterogeneity

Received 14 December 2016; Revised 13 January 2017; Accepted 24 January 2017

Introduction

Glioblastoma is the most common and aggressive primary brain tumor in adults with a median survival of only 14 months despite the best available treatments.[1] It is among the most vascularized of all solid tumors and characterized by its resistance to therapies.[2] Glioma-associated neovascularization is highly defective, resulting in a disorganized, abundant and aberrant vasculature with tortuous vessels of variable diameter and heterogeneous distribution,[3] abnormal capillary bed topology, arteriovenous shunting, microthromboses, etc.[4] This causes heterogeneity in blood flow and perfusion through the tumor vasculature and consequently impairs the delivery of nutrients, oxygen as well as therapeutics to tumor tissue.[4–6]

[1]Department of Neurosurgery, University of Erlangen-Nürnberg, Erlangen, Germany
[2]Institute of Medical Radiology, University Clinic of St. Pölten, St. Pölten, Austria
[3]Center of Functionally Integrative Neuroscience and MIND Lab, Institute of Clinical Medicine, Aarhus University, Aarhus, Denmark
[4]Department of Neuroradiology, University of Erlangen-Nürnberg, Erlangen, Germany
[5]Department of Neurology, University Clinic of St. Pölten, St. Pölten, Austria

Corresponding author:
Andreas Stadlbauer, Department of Neurosurgery, University of Erlangen-Nürnberg, Schwabachanlage 6, Erlangen 91054, Germany.
Email: andi@nmr.at

Jespersen and Østergaard[7] extended the classic flow-diffusion equation to theoretically describe the effects of capillary flow patterns on brain oxygenation introducing capillary transit time heterogeneity (CTH) as an index to account for the distribution of microvascular flow patterns.[7] A review of the putative effects of elevated CTH as a result of changes in capillary morphology in tumors suggested that elevated CTH may reduce tissue oxygen availability.[8] Recently, it became possible to estimate vascular transit time heterogeneity (VTH) in terms of the CTH index based on dynamic susceptibility contrast (DSC) magnetic resonance imaging (MRI) data using the extended model equation.[9,10] This approach has proved robust across realistic signal-to-noise ratios[9–11] and demonstrated usefulness in patients with glioma,[10,12,13] acute stroke,[9] and bilateral high-grade internal carotid artery stenosis.[14]

These studies, however, used a gradient-echo (GE) echo-planar imaging (EPI) DSC-MRI perfusion sequence. The GE-EPI DSC-MRI technique is the method of choice for routine clinical applications of DSC because of its relatively high contrast-to-noise ratio. It is well-known, however, that GE-EPI is equally sensitive to a broad range of (macro)vessel diameters (starting from 20 μm),[15] with reduced sensitivity to the microvascular range.[16] In contrast, despite its lower overall sensitivity to contrast agent-induced signal variations, spin-echo EPI (SE-EPI) DSC-MRI exhibits a peak sensitivity to the microvasculature at a vessel diameter around 10 μm,[15] including arterioles, capillaries, and venules. These differences in sensitivity to the vascular properties were shown in simulations studies[15,17] and verified in practice.[18]

Hypoxia is of crucial importance in tumor biology and therefore has the potential as a key imaging biomarker for illumination of pathophysiological mechanisms including therapy resistance and recurrence. Most of the available techniques, however, are not well suited for in vivo characterization of hypoxia in humans due to their invasiveness (electrodes), limited availability (PET), or low spatial resolution (NIR spectroscopy). An MRI-based multiparametric quantitative blood oxygenation level dependent (qBOLD) approach was recently proposed to obtain quantitative oxygenation information, namely oxygen extraction fraction and metabolic rate of oxygen.[19] MR-based assessment of tissue oxygen tension, however, was not assessable in humans so far.

The aim of this study was to introduce two MRI methods for assessment of physiological parameters: (i) mapping of transit time heterogeneity in the microvasculature with SE-EPI DSC-MRI data (termed "VTH mapping") and (ii) mapping of the oxygen tension in tissue surrounding mitochondria ($PO2_{mit}$). These MRI techniques were used to investigate whether there are differences between macro- and microvascular transit time heterogeneity (MVTH and μVTH) and oxygen tension in newly-diagnosed and recurrent glioblastoma.

Materials and methods

Patients

The institutional review boards of the University of Erlangen (263_15 Bc) and the University Clinic of St. Pölten (GS1-EK-4/339-2015) approved this retrospective study. All patients gave written informed consent in accordance with the ethical standards of the Helsinki Declaration of 1975 and its later amendments. Written consent was obtained from all enrolled patients. Using an institutional database, we retrospectively identified patients with newly-diagnosed (untreated) or recurrent glioblastoma (World Health Organization [WHO] grade IV) who were diagnosed between July 2015 and September 2016. Inclusion criteria for our study were as follows: (i) aged ≥18 years; (ii) MR scans using our study MRI protocol available; (iii) pathologically confirmed glioblastoma based on the WHO histological grading system. Additional criteria for patients with recurrent glioblastoma only were as follows: (iv) patients were previously treated according to standard of care, which included maximal safe resection, radiotherapy, and concomitant and adjuvant chemotherapy with temozolomide;[20] (v) patients who received bevacizumab or alternative chemotherapy regimens as part of their initial treatment regimen (i.e., before tumor recurrence) were excluded; and (vi) recurrence was determined by at least two board-certified radiologists in consensus based on the updated Response Assessment in Neuro-Oncology (RANO) criteria[21] with clear radiological features of recurrence.

MR image acquisition

MRI examinations were performed on a 3 Tesla clinical scanner (Tim Trio, Siemens, Erlangen, Germany) equipped with a standard 12-channel head coil. The MRI protocol included the following sequences: (i) axial fluid-attenuated inversion-recovery (FLAIR; TR/TE/TI: 5000/460/1800 ms; in-plane resolution: 0.45×0.45 mm, slice thickness: 3 mm; 48 slices; 2 averages); (ii) a single-shot diffusion-weighted echo-planar imaging (DW-EPI) sequence (TR/TE: 5300/98 ms; in-plane resolution: 1.2×1.2 mm, slice thickness: 4 mm; 29 slices; 4 averages; parallel imaging using generalized autocalibrating partially parallel acquisition (GRAPPA) factor of 2, b-values of 0 and 1000 s/mm^2); and (iii) pre- and post-contrast enhanced T1-weighted GE MRI sequences (TR/TE: 250/2.8 ms;

in-plane resolution: 0.5 × 0.5 mm, slice thickness: 4 mm; 29 slices; 2 averages).

For qBOLD we performed (iv) a multi-echo GE-, and (v) a multi-echo SE-sequence for R_2*- (8 echoes; TE, 5–40 ms; acquisition time [TA], 1.5 min) and R_2-mapping (8 echoes; TE, 13–104 ms; TA, 3.5 min), respectively.

For the VTH mapping experiments, we used (vi) a SE-EPI DSC perfusion sequence (TR, 1740 ms; TE, 33 ms; TA, 2 min) and a GE-EPI DSC perfusion sequence (TR, 1740 ms; TE, 22 ms; TA, 2 min), respectively, in combination with a dual contrast agent injections approach.[22,23] Both DSC perfusion examinations were performed with 60 dynamic measurements and administration of 0.1 mmol/kg-bodyweight gadoterate-meglumine (Dotarem, Guerbet, Aulnay-sous-Bois, France) at a rate of 4 ml/s using a MR-compatible injector (Medrad Spectris, Bayer, Leverkusen, Germany). A 20-ml-bolus of saline was injected subsequently at the same rate. Geometric parameters were chosen identical for the four qBOLD and CTH sequences: in-plane resolution: 1.8 × 1.8 mm, slice thickness: 4 mm; 29 slices; GRAPPA factor of 2.

MR image data processing

Post-processing of SE-EPI and GE-EPI DSC-MRI data was performed using the Perfusion Graphical User Interface (PGUI, http://www.cfin.au.dk/software/pgui) developed in Matlab (Mathworks, Natick, MA, USA), which implements DSC-MRI data analysis for VTH estimation using the extended flow-diffusion equation as described previously.[7] In short, the probability density function of vascular transit times h(t) is modeled by a gamma variate distribution with parameters α and β, according to

$$h(t|\alpha,\beta) = -\frac{d[1-H(t)]}{dt} = -\frac{dR(t)}{dt} = t^{\alpha-1}e^{-t/\beta}$$

where $R(t) = 1 - H(t)$ is the residue function and $H(t)$ is the distribution function of the standard microvascular model.[11,24] The contrast agent mean transit time (MTT) of a gamma variate is given by $\mathrm{MTT} = \alpha \cdot \beta$, while VTH can be quantified by the standard deviation of the gamma variate, $\mathrm{VTH} = \beta \cdot \sqrt{\alpha}$.[25]

Since we obtained two sets of parameters (for SE-EPI and GE-EPI DSC-MRI data), we adopted their nomenclature: (i) for GE-EPI DSC-MRI data which were equally sensitive to a broad range of (macro) vessel diameters we used MVTH and MMTT, and (ii) for SE-EPI DSC-MRI data which had a peak sensitivity to the microvasculature (including arterioles, capillaries, and venules), we used μVTH and μMTT, respectively.

In a next step, color-coded maps of MVTH, MMTT, μVTH, and μMTT were calculated. Because of the inherent properties of vascular networks[26] VTH and MTT as well as μVTH and μMTT values are linearly correlated in normal brain tissue, but in glioma, prior studies have shown that this relationship is disturbed and calculated the coefficient of variation (MCOV and μCOV) as the MVTH/MMTT and μVTH/μMTT ratio, respectively.[12,13] Therefore, we additionally generated MCOV and μCOV maps in order to visualize the disturbed MVTH-MMTT and μVTH-μMTT correlations within the tumors.

Post-processing of qBOLD data was performed using custom-made Matlab software and consisted of three steps: (i) Corrections for background fields of the R_2*-mapping data[27] and for stimulated echos of the R_2-mapping data.[28] (ii) Calculation of R_2*- and R_2-maps from the multi-echo relaxometry data, and of absolute cerebral blood volume (CBV) and flow (CBF) maps from the GE-EPI DSC perfusion MRI data via automatic identification of arterial input functions (AIFs) from the signal of voxels containing a large artery.[29,30] (iii) Calculation of maps for oxygen extraction fraction (OEF), cerebral metabolic rate of oxygen ($\mathrm{CMRO_2}$),[19] and the average mitochondrial oxygen tension ($\mathrm{PO2_{mit}}$)[31,32] using the following equations

$$OEF = \frac{R_2^* - R_2}{k \cdot CBV}$$

where $k = 4/3 \cdot \pi \cdot \gamma \cdot \Delta\chi \cdot \mathrm{Hct} \cdot \mathrm{B_0}$ ($\gamma = 2.67502 \cdot 10^8$ rad/s/T is the nuclear gyromagnetic ratio; $\Delta\chi = 0.264 \times 10^{-6}$ is the difference between the magnetic susceptibilities of fully oxygenated and fully deoxygenated haemoglobin; $\mathrm{Hct} = 0.42 \cdot 0.85$ is the microvascular hematocrit fraction)

$$CMRO_2 = OEF \cdot CBF \cdot C_a$$

where $C_a = 8.68$ mmol/ml is the arterial blood oxygen content[33]

$$PO2_{mit} = P_{50}\left(\frac{2}{OEF} - 1\right)^{1/h} - \frac{CMRO_2}{L}$$

where P_{50} is the hemoglobin half-saturation tension of oxygen (27 mmHg) and h is the Hill coefficient of oxygen binding to hemoglobin (2.7), and L (4.4 mmol/hg per minute) is the tissue oxygen conductivity as defined by Vafaee and Gjedde.[34]

Quantitative analysis

For quantitative analysis, the mean values for MVTH, MMTT, MCOV, μVTH, μMTT, μCOV, and $\mathrm{PO2_{mit}}$

within four regions of interest (ROI) were calculated. These ROIs were manually defined for each patient based on features seen in the FLAIR and the contrast-enhanced T1-weighted images, respectively. ROIs were located in: (i) tumor core (enhancing tumor region on contrast enhanced (CE) T1-weighted MRI) excluding necrotic parts thoroughly; (ii) peritumoral edema; (iii) ipsilateral and (iv) contralateral normal appearing brain tissue (iNAB and cNAB) of predominantly white matter.

Statistics

Software (SPSS 14, IBM, Chicago, IL, USA) was used for statistical evaluation. Differences in parameters between tumor and the other brain regions were determined using analysis of variance (ANOVA) and a Dunnett-T3 test as post hoc procedure to be consistent with (i) the unmet assumption of homogeneity of variance and (ii) as correction for multiple comparisons. Homogeneity of variance was tested using the Levene's test. A Wilcoxon signed-rank test was used for comparisons between MVTH, MMTT, and MCOV values from GE-EPI DSC data and μVTH, μMTT, and μCOV values from SE-EPI DSC perfusion data, i.e. between macro- and microvasculature. A Mann–Whitney test was used for comparison of VTH mapping parameters and oxygen tension values between newly-diagnosed and recurrent glioblastoma. Regression analyses with a linear model (two parameters) and a quadratic polynomial model (three parameters) were performed for correlations between MVTH vs. MMTT and μVTH vs. μMMT. An F-test was used to check for significance of differences in correlation coefficients between the models. *P*-values less than 0.05 were considered to indicate significance.

Results

In total, 57 patients with newly-diagnosed (untreated) or recurrent glioblastoma were included in this study based on our criteria. Twenty-five patients (10 women, 15 men; mean age ± standard deviation, 64.8 ± 11.9 years) suffered from a newly-diagnosed glioblastoma, and 32 patients (16 women, 16 men; 63.3 ± 9.7 years) from a recurrent glioblastoma, respectively. All patients with recurrent glioblastoma received the Stupp protocol.[20] Nine patients, however, received less than six cycles temozolomide (3–5 cycles) due to side effects. Representative cases for VTH mapping of the macro- and microvasculature in patients with newly-diagnosed and recurrent glioblastoma are depicted in Figure 1(a) and (b), respectively. The findings for the 25 patients with newly-diagnosed glioblastoma and the 32 patients with recurrent glioblastoma are summarized in Table 1.

Differences in VTH mapping between glioblastoma and normal brain

As expected and described previously, VTH mapping parameters derived from GE-EPI DSC-MRI data (i.e. for macrovasculature; MVTH, MMTT, and MCOV) of glioblastoma were increased compared to normal brain (second column in Figure 1). However, only for recurrent glioblastoma were these differences to normal brain significant (all $P < 0.05$), except for MMTT, which was not significantly different to iNAB. The differences between newly-diagnosed glioblastoma and normal brain for the VTH mapping parameters in the macrovasculature did not reach significance (upper part of Table 1).

On the other hand, μVTH and μMTT for the microvasculature of both newly-diagnosed and recurrent glioblastoma were significantly increased (for all $P \leq 0.001$) compared to normal brain. Nevertheless, μCOV values, i.e. the μVTH/μMTT ratios, were significantly decreased (for all $P \leq 0.001$) in both newly-diagnosed and recurrent glioblastoma compared to normal brain (middle part of Table 1).

In other words, the relative vascular transit time heterogeneity was increased in the macrovasculature (MCOV) but decreased in the microvasculature (μCOV) of glioblastoma compared to normal brain (third column in Figure 1).

Differences in VTH mapping between macro- and microvasculature

In microvasculature, μVTH and μMTT were significantly larger ($P = 0.011$ to <0.001) compared to their equivalents in macrovasculature (MVTH and MMTT) for all ROIs in patients with both newly-diagnosed and recurrent glioblastoma.

The value for μCOV in normal brain (iNAB and cNAB) and edema were also significantly larger ($P = 0.024$ to 0.001) compared to macrovasculature (MCOV). Within newly-diagnosed and recurrent glioblastoma, however, μCOV was significantly lower (both $P < 0.001$) compared to MCOV. In other words, in glioblastoma, the relative transit time heterogeneity in the microvasculature was significantly lower than in the macrovasculature (compare second and third column in Figure 1, or third and sixth row in Table 1).

Differences between newly-diagnosed and recurrent glioblastoma

Recurrent glioblastoma showed significantly increased μVTH ($P = 0.014$; Figure 2(a)) and μCOV values ($P = 0.039$; Figure 2(c)) compared to newly-diagnosed

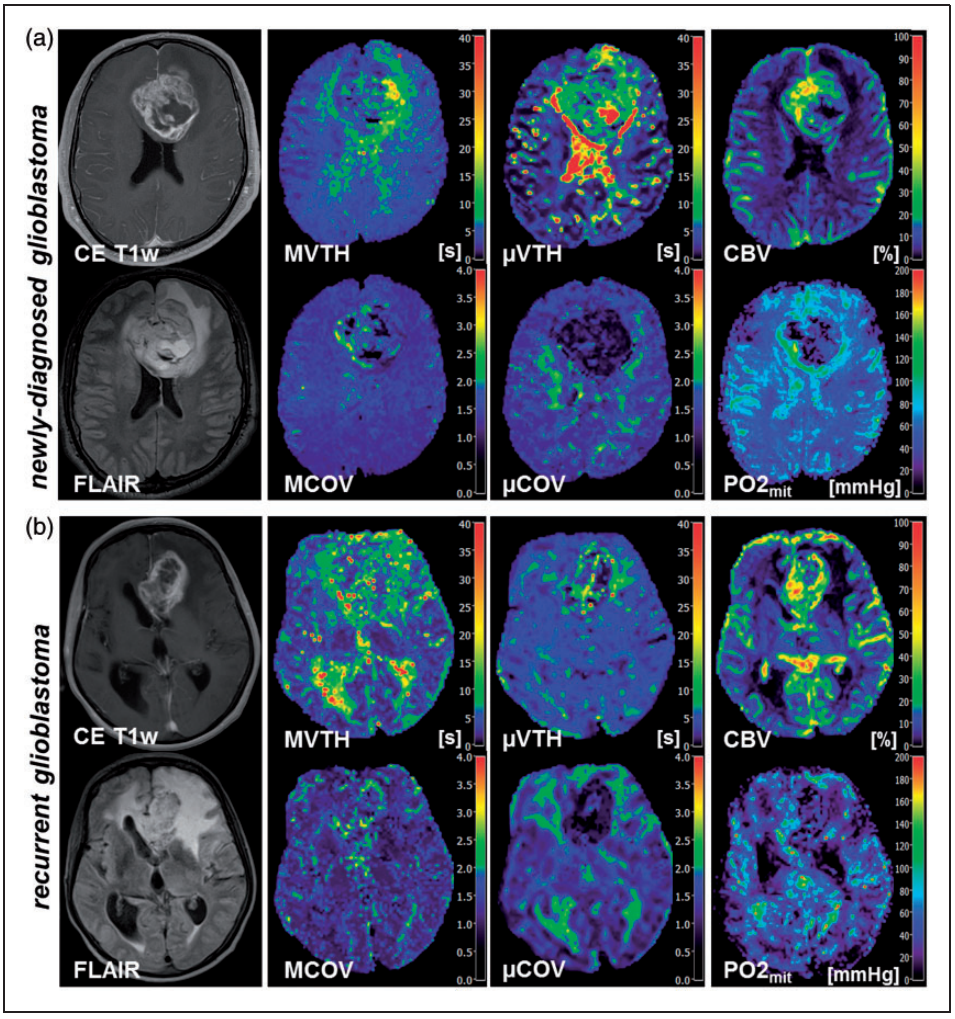

Figure 1. VTH mapping of the macro- and microvasculature and $PO2_{mit}$ mapping in (a) a 46-year-old male patients suffering from a newly-diagnosed glioblastoma and (b) a 63-year-old female patients suffering from a recurrent glioblastoma. First column, contrast-enhanced T1-weighted (CE T1w) MR images and FLAIR MR images. Second column, results for VTH mapping using GE-EPI DSC-MRI data in order to obtain maps of macrovascular VTH (MVTH) and coefficient of variation (MCOV). Third column, results for VTH mapping using SE-EPI DSC-MRI data in order to obtain maps of microvascular VTH (μVTH) and coefficient of variation (μCOV). Last column, maps of absolute cerebral blood volume (CBV) obtained from GE-EPI DSC-MRI data and oxygen tension in tissue surrounding mitochondria ($PO2_{mit}$).

glioblastoma. For μMTT, we also found higher values in recurrent glioblastoma which, however, did not reach significance ($P = 0.162$; Figure 2(b)). This was associated with significantly decreased ($P = 0.008$) $PO2_{mit}$ values in recurrent glioblastoma (Figure 2(d)). For VTH mapping in the macrovasculature (MVTH, MMTT, MCOV), we found no significant differences between newly-diagnosed and recurrent glioblastoma.

Correlations between transit time heterogeneities and MTTs

The correlations of MVTH vs. MMTT and μVTH vs. μMTT for the subgroups of patients with newly-diagnosed and recurrent glioblastoma are depicted in the first and second plots of Figure 3(a) and (b), respectively. The MVTH vs. MMTT correlation demonstrated a superposition for normal brain (iNAB and cNAB), edema, and tumor (first column in Figure 3). Interestingly, the μVTH vs. μMTT scatterplots showed a separation between normal brain/edema and tumor (second column in Figure 3). The third plots in Figure 3(a) and (b)give an overview for the differences in correlations between macro- and microvasculature in newly-diagnosed and recurrent glioblastoma, respectively.

Regression analyses between MVTH vs. MMTT and μVTH vs. μMTT generally revealed better correlations for the more complex model (quadratic polynomial with three parameters) compared to the more restricted

Table 1. Overview of the quantitative evaluation of the VTH mapping parameters, $PO2_{mit}$ and perfusion values.

	GB type	Tumor	Edema	iNAB	cNAB
MVTH	Newly-diagn.	5.72 ± 2.12	6.34 ± 2.99	4.68 ± 1.58	4.48 ± 1.52
[s]	Recurrent	6.13 ± 1.78	5.89 ± 1.89	4.64 ± 1.71*	4.60 ± 1.65*
MMTT	Newly-diagn.	4.71 ± 1.70	5.12 ± 2.36	3.97 ± 1.27	3.82 ± 1.15
[s]	Recurrent	4.78 ± 1.21	5.21 ± 1.80	3.96 ± 1.41	3.86 ± 1.38*
MCOV	Newly-diagn.	1.22 ± 0.16	1.23 ± 0.11	1.16 ± 0.10	1.16 ± 0.12
	Recurrent	1.29 ± 0.14	1.17 ± 0.10*	1.17 ± 0.12*	1.19 ± 0.11*
μVTH	Newly-diagn.	12.25 ± 5.22	10.66 ± 5.14	6.78 ± 3.08**	6.51 ± 2.56**
[s]	Recurrent	16.23 ± 6.51	10.36 ± 3.09**	7.20 ± 2.59**	6.61 ± 1.57**
μMTT	Newly-diagn.	15.55 ± 7.62	8.68 ± 4.88**	5.07 ± 2.45**	5.12 ± 2.29**
[s]	Recurrent	18.65 ± 8.57	8.20 ± 2.69**	5.50 ± 2.42**	5.03 ± 1.63**
μCOV	Newly-diagn.	0.81 ± 0.15	1.30 ± 0.20**	1.36 ± 0.21**	1.33 ± 0.22**
	Recurrent	0.90 ± 0.14	1.40 ± 0.26**	1.37 ± 0.33**	1.36 ± 0.30**
$PO2_{mit}$	Newly-diagn.	20.3 ± 10.6	38.8 ± 7.9**	26.8 ± 5.3	26.6 ± 4.9
[mmHg]	Recurrent	13.0 ± 8.2	42.4 ± 7.5**	29.1 ± 8.7**	29.3 ± 9.3**
CBV	Newly-diagn.	25.3 ± 8.6	2.5 ± 0.9**	4.5 ± 0.9**	4.4 ± 0.8**
[%]	Recurrent	22.6 ± 9.2	2.8 ± 0.9**	4.4 ± 0.8**	4.6 ± 0.8**
CBF	Newly-diagn.	63.9 ± 19.3	13.5 ± 6.6**	26.1 ± 6.3**	25.4 ± 5.5**
[ml/100 g/min]	Recurrent	68.2 ± 16.9	18.8 ± 6.9**	26.1 ± 5.9**	26.0 ± 5.7**

*Values are significant different to tumor with $P < 0.05$. **Values are significant different to tumor with $P \leq 0.001$. GB: glioblastoma; Newly-diagn.: newly-diagnosed (untreated) glioblastoma; MVTH: macrovascular transit time heterogeneity; MMTT: macrovascular mean transit time; COV: macrovascular coefficient of variation (MVTH/MMTT) for; μVTH: microvascular transit time heterogeneity; μMTT: microvascular mean transit time in; μCOV: microvascular coefficient of variation (μVTH/μMTT); $PO2_{mit}$: oxygen tension for tissue around mitochondria; CBV: cerebral blood volume: CBF: cerebral blood flow; iNAB and cNAB: ipsilateral and contralateral normal appearing brain tissue of predominantly white matter. Perfusion parameters (CBV and CBF) were calculated from GE- and SE-DSC perfusion MRI data.

model (linear with two parameters), which was mathematically coherent. In normal appearing brain tissue (iNAB and cNAB), however, the differences in correlation coefficients between the two models were very minor (in the third digital place) and not statistically significant using an F-test. Therefore, the assumption of a linear correlation in NAB was justified. The linear correlation coefficients in NAB were as follows: MVTH vs. MMTT, $R^2 = 0.918$ (newly-diagnosed glioblastoma) and $R^2 = 0.904$ (recurrent glioblastoma); μVTH vs. μMTT; $R^2 = 0.902$ (newly-diagnosed) and $R^2 = 0.686$ (recurrent). The correlation coefficients in peritumoral edema were very similar.

The microvasculature (μVTH vs. μMTT) of recurrent glioblastoma showed a significantly stronger correlation ($P = 0.038$) for quadratic polynomial regression model ($R^2 = 0.922$) compared to the linear model ($R^2 = 0.854$). However, the differences in correlations for the microvasculature of newly-diagnosed glioblastoma and the macrovasculature (MVTH vs. MMTT) of both glioblastoma subtypes were not significant. The quadratic polynomial correlation coefficients were as follows: μVTH vs. μMTT in newly-diagnosed glioblastoma, $R^2 = 0.848$; MVTH vs. MMTT, $R^2 = 0.890$ (newly-diagnosed) and $R^2 = 0.875$ (recurrent, see third plots in Figure 3(a) and (b))

Discussion

This study introduces a physiological MRI approach including micro- and macrovascular VTH and $PO2_{mit}$ mapping. This enabled us to demonstrate that pathologic VTH alterations in glioblastoma are dominated by microvasculature (vessel diameters around 10 μm) and revealed three main findings regarding the pathophysiology of glioblastoma: (i) the relative VTH was decreased in microvasculature (μCOV) but increased in macrovasculature (MCOV) compared to the other brain regions (iNAB, cNAB, and edema); (ii) recurrence of glioblastoma was associated with elevated microvascular perfusion dispersion (μVTH, μCOV) and (iii) increased hypoxia (decreased $PO2_{mit}$) compared to newly-diagnosed glioblastoma.

Firstly, the finding of decreased μCOV values in glioblastoma was remarkable and unexpected. With μCOV values <1.0 in both newly-diagnosed and recurrent glioblastoma and μCOV ≥ 1.3 in other brain regions, the differences were distinct and significant. MCOV values, however, were increased within the lesions. To the best of our knowledge, the investigation of VTH using the SE-DSC perfusion MRI technique, which is more sensitive to the microvasculature, in patients with glioblastoma has been not described

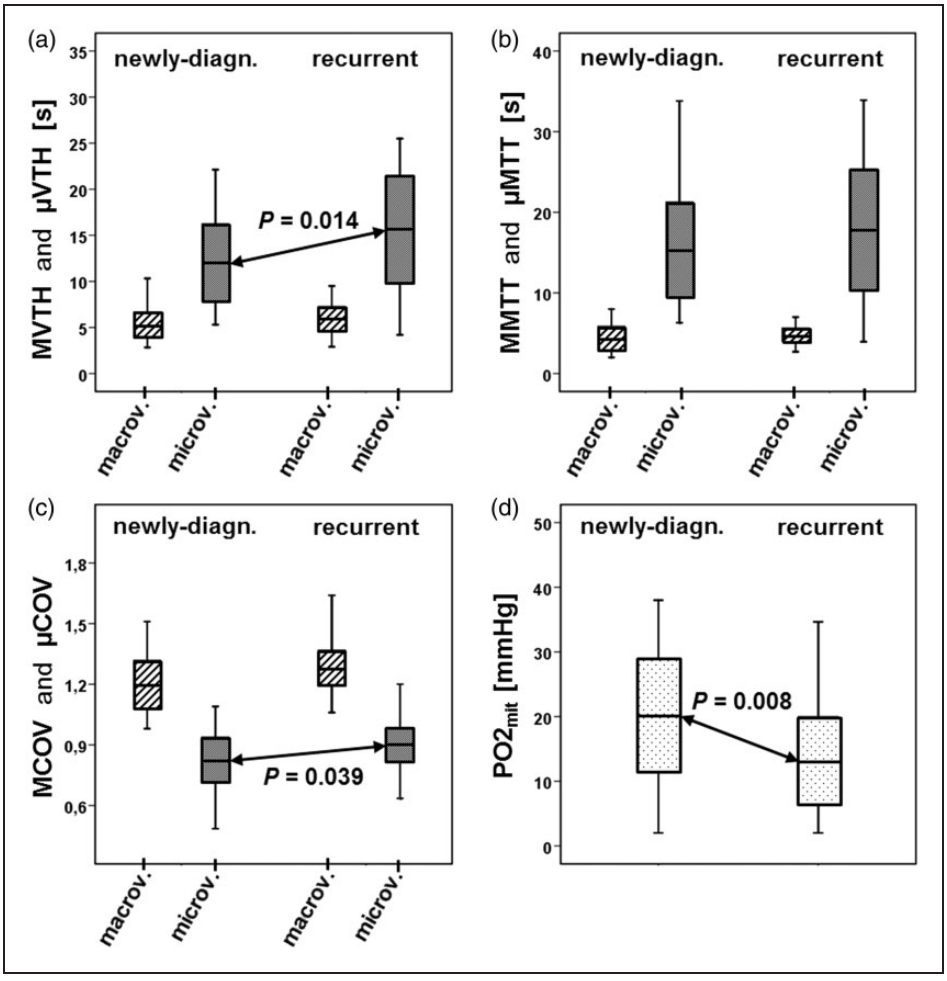

Figure 2. Box-whisker plots (whiskers: minimum, maximum; box: 25th to 75th percentile; line: mean value) VTH mapping parameters and the $PO2_{mit}$ values of all patients with newly-diagnosed glioblastoma (N = 25) and recurrent glioblastoma (N = 32). (a) macrovascular and microvascular VTH (MVTH and µVTH) within newly-diagnosed (left part) and recurrent glioblastoma (right part). µVTH was significant higher ($P = 0.014$) in recurrent glioblastoma compared to newly-diagnosed glioblastoma. (b) macrovascular and microvascular MTT (MMTT and µMTT) within newly-diagnosed (left part) and recurrent glioblastoma (right part). MMTT was increased in recurrent glioblastoma but reached not statistical significance. (c) macrovascular and microvascular COV (MCOV and µCOV) within newly-diagnosed (left part) and recurrent glioblastoma (right part). µCOV was significant higher ($P = 0.039$) in recurrent glioblastoma compared to newly-diagnosed glioblastoma. (d) oxygen tension in tissue surrounding mitochondria ($PO2_{mit}$) within newly-diagnosed (left part) and recurrent glioblastoma (right part). $PO2_{mit}$ was significant lower ($P = 0.008$) in recurrent glioblastoma compared to newly-diagnosed glioblastoma. Macrov: macrovasculature; microv: microvasculature.

so far. Our findings regarding increased µVTH and µMTT, however, are in line with the theoretical considerations of a review about the putative effects of changes in capillary morphology in tumors.[8] Although both µVTH and µMTT are markedly increased compared to normal brain, the low µCOV (i.e. µVTH/µMTT ratio) values indicate a decrease in µVTH (standard deviation of transit time distribution) relative to µMTT (mean value of transit time distribution). This may provide evidence for a mechanism of adaption of microvasculature to retain the high metabolic demands of the lesion within a disorganized and inefficient vasculature. Our findings for the transit time heterogeneity in the macrovasculature of glioblastoma are in accordance with previous studies using the standard GE-DSC perfusion MRI technique which have shown that the relationship between MMTT and MVTH is altered, resulting in elevation of the MCOV values.[12,13] The differences in micro- and macrovascular VTH mapping were supported by our regression analyses, which confirmed, on the one hand, the common assumption[13] of a linear correlation between VTH and MTT in the normal micro- and macrovascular bed. On the other hand, we revealed significant differences for the correlations between micro- and macrovasculature in glioblastoma. This may be

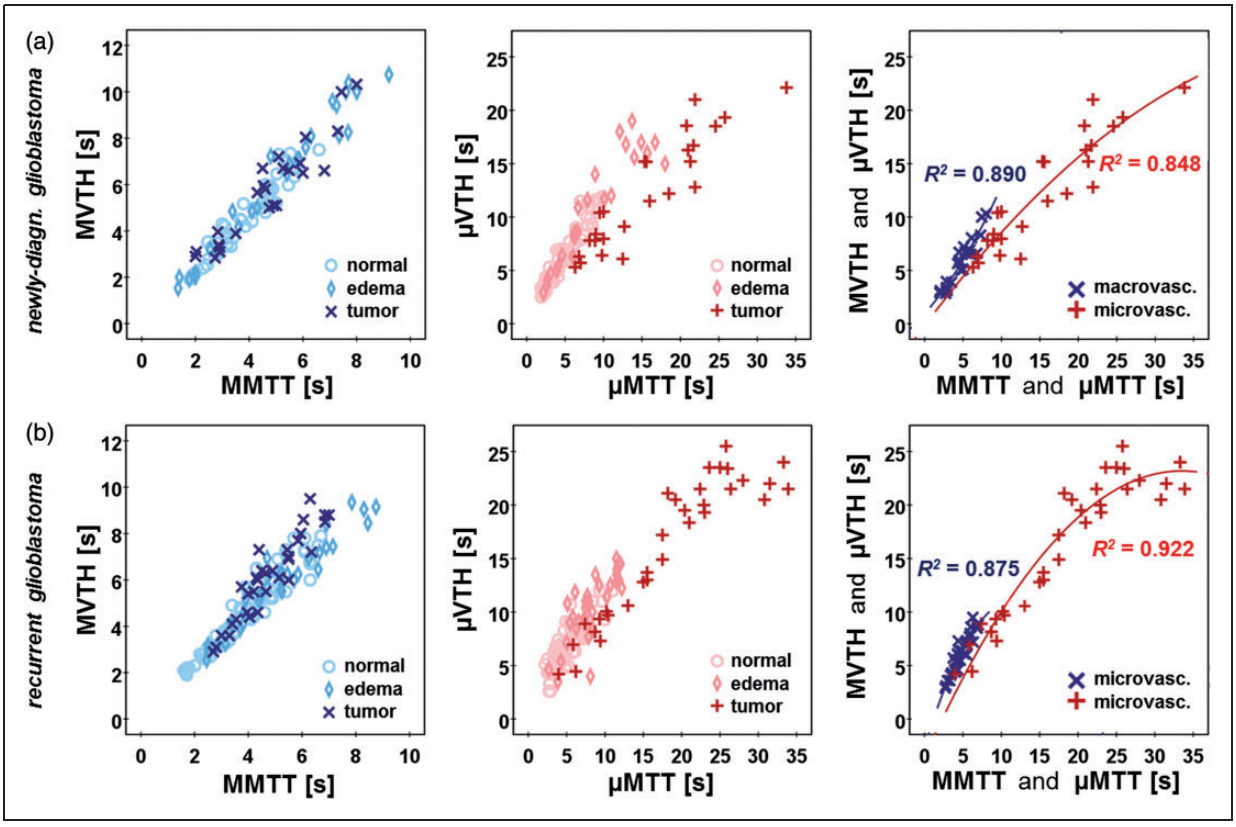

Figure 3. Scatterplots of VTHs versus MTTs for all patients with (a) newly-diagnosed glioblastoma (N = 25) and (b) recurrent glioblastoma (N = 32). First column, the scatterplots of macrovascular VTH versus MTT (MVTH vs. MMTT) for normal brain regions (iNAB and cNAB; circles), peritumoral edema (diamonds), and tumor (crosses) show a strong linear correlation and superposition for all four ROIs. Second column, the scatterplots macrovascular VTH versus MTT (μVTH vs. μMTT) showed a separation between normal brain (circles), edema (diamonds), and tumor (crosses). Last column, comparison of scatterplot between macro- and microvasculature (MVTH vs. MMTT and μVTH vs. μMTT) in newly-diagnosed (a) and recurrent glioblastoma (b).

interpreted as a further evidence for decoupling of μVTH and μMTT in glioblastomas.

Secondly, we revealed that recurrent glioblastoma showed significantly increased perfusion dispersion in the microvasculature (μVTH, μCOV) compared to newly-diagnosed glioblastoma. This is an indication for stress response of the microvascular network in failed-therapy glioblastoma in order to protect tumor cells by an intact neurovascular unit,[35] which was already suggested by the observations of previous studies.[12,36] A close association between endothelial cells and neural stem cells was demonstrated in a seminal work of Shen et al.[37] They found that endothelial cells secrete factors that stimulate self-renewal of neural stem cells and proposed that endothelial cells are an integral component of the stem cell niche. This vascular niche has also been applied to glioblastoma stem cells.[38,39] It can be thought of as protective microenvironment in which glioblastoma stem cells are able to freely proliferate and remain undifferentiated, completely unaffected by any external influences.[38,39] Moreover, a combined effect of high VTH and blood flow was predicted to be associated with insufficient oxygen extraction and hypoxia.[7] This was supported with patient data demonstrating an increased expression of hypoxia markers in tissue regions with altered capillary transit times.[40]

Finally, our finding of significantly decreased $PO2_{mit}$ in failed-therapy glioblastoma compared to both normal brain tissue and newly-diagnosed glioblastoma is in accordance with the well-known role of hypoxia in therapy resistance of glioblastoma. Tumor progression and resistance to both radiotherapy and chemotherapy are associated with a hypoxic tumor microenvironment known as hypoxic niche.[1,41,42] Hypoxia promotes a more malignant phenotype of cancer cells and supports the survival of glioma stem cells which possess greater drug resistance, self-renewal potential and tumorigenicity.[43–45] Our data support the assumption for an association between the vascular and the hypoxic niche. Tumor-initiating stem cells thrive in hypoxic environments which are localized in peri-capillary niches where

the aberrant capillary networks appear to offer optimal conditions for tumor maintenance, as well as therapy resistance.[38,39]

This study has several limitations. There is no clear benefit for the routine clinical management of patients of the demonstrated differences in vascular heterogeneity and $PO2_{mit}$ between newly-diagnosed and recurrent glioblastoma. However, our approach may be helpful for therapy monitoring or to develop new therapeutic strategies for glioblastoma. Furthermore, biological validation of the MR-based parameters for vascular transit time heterogeneity and tissue oxygen tension is required by correlation with findings from immunohistochemistry of biopsies, results from examinations using invasive methods,[46,47] or data from other imaging modalities (e.g. positron emission tomography).[48] Thereby, the link between the mathematical models of our approach and biology could be understood in more detail. The $PO2_{mit}$ values in newly-diagnosed and recurrent glioblastoma are quite high compared to data from studies using invasive methods.[49] A reason for this might be the fact that $PO2_{mit}$ in our study is a derived parameter based on MR experiments with a lower spatial resolution compared to invasive, more direct methods.[49] The SE-DSC perfusion sequence has lower contrast to noise compared to the GE-DSC approach. This is related to the generally lower sensitivity to magnetic susceptibility of SE MRI sequences compared to the highly susceptibility-sensitive GE sequences. However, this different sensitivity to magnetic susceptibility is the crucial reason for their vessel-size-dependence. Additionally, the injection of a double dose of contrast agent with two separate injections is required. A combined GE-SE perfusion sequence with the Simultaneous-MultiSlice (SMS) technique may help to overcome this limitation.[50] Finally, our $PO2_{mit}$ mapping approach needs validation with invasive methods in animal models.

In conclusion, μVTH and $PO2_{mit}$ mapping provides potential imaging biomarkers for investigation of physiological and metabolic alterations in glioblastoma including the vascular and hypoxic niche, which are responsible for tumor progression and therapy resistance of glioblastoma. However, further studies including patients with anaplastic and low-grade glioma, pseudo-progression, and under anti-angiogenetic or more advanced therapies are required.

Funding

The author(s) disclosed receipt of the following financial support for the research, authorship, and/or publication of this article: This work was supported by the German Research Foundation (Deutsche Forschungsgemeinschaft – DFG; Grant Numbers STA 1331/3-1 and DO 721/8-1) and by the ELAN program (Erlanger Leistungsbezogene Anschubfinanzierung und Nachwuchsförderung; Grant Number 14-05-21-1-Stadlbauer).

Declaration of conflicting interests

The author(s) declared no potential conflicts of interest with respect to the research, authorship, and/or publication of this article.

Authors' contributions

AS, GH, AD, MB and KR conceived the study. AS, MBH and MZ involved in analysis of data. KM, MBH, AS and MZ contributed to the development of the software tools for calculation of MRI biomarkers. KM, MBH, AS, GH, AD and KR involved interpretation of data. AS, GH, and SO contributed to acquisition of data. All authors reviewed the manuscript critically for intellectual content, and read and approved the final manuscript.

References

1. Hardee ME and Zagzag D. Mechanisms of glioma-associated neovascularization. *Am J Pathol* 2012; 181: 1126–1141.
2. Takano S, Yamashita T and Ohneda O. Molecular therapeutic targets for glioma angiogenesis. *J Oncol* 2010; 351908: 1–11.
3. Dvorak HF. How Tumors make bad blood vessels and stroma. *Am J Pathol* 2016; 162: 1747–1757.
4. Pries AR, Hopfner M, le Noble F, et al. The shunt problem: Control of functional shunting in normal and tumour vasculature. *Nat Rev Cancer* 2010; 10: 587–593.
5. Jain RK, Di Tomaso E, Duda DG, et al. Angiogenesis in brain tumours. *Nat Rev Neurosci* 2007; 8: 610–622.
6. Carmeliet P and Jain RK. Angiogenesis in cancer and other diseases. *Nature* 2000; 407: 249–257.
7. Jespersen SN and Østergaard L. The roles of cerebral blood flow, capillary transit time heterogeneity, and oxygen tension in brain oxygenation and metabolism. *J Cereb Blood Flow Metab* 2012; 32: 264–277.
8. Østergaard L, Tietze A, Nielsen T, et al. The Relationship between tumor blood flow, angiogenesis, tumor hypoxia, and aerobic glycolysis. *Cancer Res*. 2013; 73: 5618–5624.
9. Mouridsen K, Hansen MB, Østergaard L, et al. Reliable estimation of capillary transit time distributions using DSC-MRI. *J Cereb Blood Flow Metab* 2014; 34: 1511–21.
10. Hansen MB, Tietze A, Kalpathy-Cramer J, et al. Reliable estimation of microvascular flow patterns in patients with disrupted blood–brain barrier using dynamic susceptibility contrast MRI. *J Magn Reson Imaging* 2017; (in-press).
11. Mouridsen K, Friston K, Hjort N, et al. Bayesian estimation of cerebral perfusion using a physiological model of microvasculature. *Neuroimage* 2006; 33: 570–579.
12. Bonekamp D, Mouridsen K, Radbruch A, et al. Assessment of tumor oxygenation and its impact on treatment response in bevacizumab-treated recurrent glioblastoma. *J Cereb blood flow Metab* 2017; 37: 485–494.
13. Tietze A, Mouridsen K, Lassen-Ramshad Y, et al. Perfusion MRI derived indices of microvascular shunting and flow control correlate with tumor grade and outcome in patients with cerebral glioma. *PLoS One* 2015; 10: 1–16.

14. Mundiyanapurath S, Ringleb PA, Diatschuk S, et al. Capillary transit time heterogeneity is associated with modified rankin scale score at discharge in patients with bilateral high grade internal carotid artery stenosis. *PLoS One* 2016; 11: 1–10.
15. Boxerman JL, Hamberg LM, Rosen BR, et al. MR contrast due to intravascular magnetic susceptibility perturbations. *Magn Reson Med* 1995; 34: 555–566.
16. Schmiedeskamp H, Straka M, Newbould RD, et al. Combined spin- and gradient-echo perfusion-weighted imaging. *Magn Reson Med* 2012; 68: 30–40.
17. Weisskoff RM, Zuo CS, Boxerman JL, et al. Microscopic susceptibility variation and transverse relaxation: Theory and experiment. *Magn Reson Med* 1994; 31: 601–610.
18. Speck O, Chang L, Menaka DeSilva N, et al. Perfusion MRI of the human brain with dynamic susceptibility contrast: Gradient-echo versus spin-echo techniques. *J Magn Reson Imaging* 2000; 12: 381–387.
19. Christen T, Schmiedeskamp H, Straka M, et al. Measuring brain oxygenation in humans using a multiparametric quantitative blood oxygenation level dependent MRI approach. *Magn Reson Med* 2012; 68: 905–911.
20. Stupp R, Hegi ME, Mason WP, et al. Effects of radiotherapy with concomitant and adjuvant temozolomide versus radiotherapy alone on survival in glioblastoma in a randomised phase III study: 5-year analysis of the EORTC-NCIC trial. *Lancet Oncol* 2009; 10: 459–466.
21. Wen PY, Macdonald DR, Reardon DA, et al. Updated response assessment criteria for high-grade gliomas: Response assessment in neuro-oncology working group. *J Clin Oncol* 2010; 28: 1963–1972.
22. Stadlbauer A, Zimmermann M, Heinz G, et al. Magnetic resonance imaging biomarkers for clinical routine assessment of microvascular architecture in glioma. *J Cereb Blood Flow Metab* 2017; 37: 632–643.
23. Hsu Y-Y, Yang W-S, Lim K-E, et al. Vessel size imaging using dual contrast agent injections. *J Magn Reson Imaging* 2009; 30: 1078–84.
24. Østergaard L, Weisskoff RM, Chesler DA, et al. High resolution measurement of cerebral blood flow using intravascular tracer bolus passages. Part I: Mathematical approach and statistical analysis. *Magn Reson Med* 1996; 36: 715–725.
25. Thompson HK, Starmer CF, Whalen RE, et al. Indicator transit time considered as a gamma variate. *Circ Res* 1964; 14: 502–515.
26. Rasmussen PM, Jespersen SN and Østergaard L. The effects of transit time heterogeneity on brain oxygenation during rest and functional activation. *J Cereb Blood Flow Metab* 2015; 35: 432–442.
27. Preibisch C, Volz S, Anti S, et al. Exponential excitation pulses for improved water content mapping in the presence of background gradients. *Magn Reson Med* 2008; 60: 908–916.
28. Prasloski T, Mädler B, Xiang QS, et al. Applications of stimulated echo correction to multicomponent T2 analysis. *Magn Reson Med* 2012; 67: 1803–1814.
29. Bjornerud A and Emblem KE. A fully automated method for quantitative cerebral hemodynamic analysis using DSC-MRI. *J Cereb Blood Flow Metab* 2010; 30: 1066–1078.
30. Smith AM, Grandin CB, Duprez T, et al. Whole Brain Quantitative CBF, CBV, and MTT Measurements Using MRI Bolus Tracking: Implementation and Application to Data Acquired From Hyperacute Stroke Patients. *J Magn Reson Imaging* 2000; 12: 400–410.
31. Vafaee MS, Vang K, Bergersen LH, et al. Oxygen consumption and blood flow coupling in human motor cortex during intense finger tapping: Implication for a role of lactate. *J Cereb Blood Flow Metab* 2012; 32: 1859–1868.
32. Gjedde A, Johannsen P, Cold GE, et al. Cerebral metabolic response to low blood flow: Possible role of cytochrome oxidase inhibition. *J Cereb Blood Flow Metab* 2005; 25: 1183–1196.
33. Kennan RP, Zhong J and Gore JC. Intravascular susceptibility contrast mechanisms in tissues. *Magn Reson Med* 1994; 31: 9–21.
34. Vafaee MS and Gjedde A. Model of blood-brain transfer of oxygen explains nonlinear flow-metabolism coupling during stimulation of visual cortex. *J Cereb blood flow Metab* 2000; 20: 747–754.
35. Furnari FB, Fenton T, Bachoo RM, et al. Malignant astrocytic glioma: Genetics, biology, and paths to treatment. *Genes Dev* 2007; 21: 2683–2710.
36. Plate KH, Scholz A and Dumont DJ. Tumor angiogenesis and anti-angiogenic therapy in malignant gliomas revisited. *Acta Neuropathol* 2012; 124: 763–775.
37. Shen Q, Goderie SK, Jin L, et al. Endothelial cells stimulate self-renewal and expand neurogenesis of neural stem cells. *Science* 2004; 304: 1338–1340.
38. Gilbertson RJ and Rich JN. Making a tumour's bed: Glioblastoma stem cells and the vascular niche. *Nat Rev Cancer* 2007; 7: 733–736.
39. Calabrese C, Poppleton H, Kocak M, et al. A perivascular niche for brain tumor stem cells. *Cancer Cell* 2007; 11: 69–82.
40. Jensen RL, Mumert ML, Gillespie DL, et al. Preoperative dynamic contrast-enhanced MRI correlates with molecular markers of hypoxia and vascularity in specific areas of intratumoral microenvironment and is predictive of patient outcome. *Neuro Oncol* 2014; 16: 280–291.
41. Hsieh CH, Shyu WC, Chiang CY, et al. NADPH oxidase subunit 4-mediated reactive oxygen species contribute to cycling hypoxia-promoted tumor progression in glioblastoma multiforme. *PLoS One* 2011; 6: e23945.
42. Rong Y, Durden DL, Van Meir EG, et al. 'Pseudopalisading' necrosis in glioblastoma: A familiar morphologic feature that links vascular pathology, hypoxia, and angiogenesis. *J Neuropathol Exp Neurol* 2006; 65: 529–39.
43. Singh SK, Hawkins C, Clarke ID, et al. Identification of human brain tumour initiating cells. *Nature* 2004; 432: 396–401.
44. Bao S, Wu Q, McLendon RE, et al. Glioma stem cells promote radioresistance by preferential activation of the DNA damage response. *Nature* 2006; 444: 756–760.

45. Galli R, Binda E, Orfanelli U, et al. Isolation and characterization of tumorigenic, stem-like neural precursors from human glioblastoma. *Cancer Res* 2004; 64: 7011–7021.
46. Vajkoczy P, Schilling L, Ullrich A, et al. Characterization of angiogenesis and microcirculation of high-grade glioma: An intravital multifluorescence microscopic approach in the athymic nude mouse. *J Cereb Blood Flow Metab* 1998; 18: 510–520.
47. Villringer A, Them A, Lindauer U, et al. Capillary perfusion of the rat-brain cortex – An in-vivo confocal microscopy study. *Circ Res* 1994; 75: 55–62.
48. Valable S, Corroyer-Dulmont A, Chakhoyan A, et al. Imaging of brain oxygenation with magnetic resonance imaging: A validation with positron emission tomography in the healthy and tumoural brain. *J Cereb Blood Flow Metab* 2017; (in-press).
49. Vaupel P, Hockel M and Mayer A. Detection and characterization of tumor hypoxia using pO2 histography. *Antioxid Redox Signal* 2007; 9: 1221–1235.
50. Eichner C, Jafari-Khouzani K, Cauley S, et al. Slice accelerated gradient-echo spin-echo dynamic susceptibility contrast imaging with blipped CAIPI for increased slice coverage. *Magn Reson Med* 2013; 72: 770–778.